



3D Scaffold Designing based on Conductive/Degradable Tetrapolymeric Nanofibers of PHEMA-co-PNIPAAm-co-PCL/PANI for Bone Tissue Engineering

Raana Sarvari¹, Samira Agbolaghi^{*2}, Younes Beygi-Khosrowshahi²,
Bakhshali Massoumi¹, Ali Bahadori³

¹Department of Chemistry, Payame Noor University, Tehran, Iran.

²Chemical Engineering Department, Faculty of Engineering, Azarbaijan Shahid Madani University, Tabriz, Iran.

³University of Applied Science and Technology, Tabriz, Iran.

Received: 16 Mrch 2018; Accepted: 27 August 2018

* Corresponding author email: s.agbolaghi@azaruniv.ac.ir

ABSTRACT

The hydrophilic, conducting, biocompatible and porous scaffolds were designed using poly(2-hydroxy ethyl methacrylate)-co-poly(N-isopropylacrylamide)-co-poly(ϵ -caprolactone) (P(HEMA-*b*-NIPAAm-*b*-CL))/polyaniline (PANI) for the osteoblast applications. To this end, the PHEMA and P(HEMA-*b*-NIPAAm) were synthesized via reversible addition of fragmentation chain transfer (RAFT) polymerization, and in next step, the ϵ -caprolactone was polymerized from -OH group of PHEMA segments through the ring opening polymerization (ROP). The electroactivity, mechanical properties, and hydrophilicity of designed scaffolds played an important role in the adhesion, differentiation, and proliferation of MG63 cells. By using the PHEMA and PNIPAAm, the hydrophilicity and biocompatibility, and by employing the PCL, the appropriate mechanical properties were acquired. The addition of PANI in the composition induced the conductivity to scaffolds. The morphology, electrical conductivity, biocompatibility, hydrophilicity and mechanical characteristics of the nanofibers were thoroughly investigated. The scaffolds possessed a porous nanostructure (nanofiber diameter ranged in 60–130 nm) with a large surface area, electrical conductivity of 0.03 S cm^{-1} and contact angle of $49 \pm 5^\circ$, which imitated the natural microenvironment of extra cellular matrix (ECM) to regulate the cell attachment, proliferation and differentiation. *In vitro* cytocompatibility studies were performed over 168 h and indicated that the nanofibers were non-toxic to MG63 cells and potent to the artificial nanostructured osteoblasting.

Keywords: Scaffold, Osteoblast, Electrospun Nanofiber, Poly(2-hydroxyethylmethacrylate), Poly(N-isopropylacrylamide), Polycaprolactone.

1. Introduction

The electroactive biomaterials, including conductive polymers, electrets, piezoelectric and photovoltaic materials, are the smart materials

which allow the direct delivery of electrical, electrochemical and electromechanical stimulation to cells [1–4]. The electrets and piezoelectric materials allow the delivery of an electrical

stimulus without the need for an external power source, but the control over the stimulus is limited [4,5]. On the other side, the conductive polymers provide an excellent control over the electrical stimulus and they have very good electrical and optical properties as well as high conductivity/weight ratio [5–7]. Furthermore, a great advantage of conductive polymers is that their chemical, electrical and physical properties can be tailored to the specific needs of their application by incorporating antibodies, enzymes and other biological moieties [1,4,7,8]. These properties can be also altered and controlled through stimulation even after synthesis [9–12].

Among conductive polymers, polyaniline (PANI) exists in various forms based on its oxidation level, i.e., the fully oxidized pernigraniline base, half-oxidized emeraldine base and fully reduced leucoemeraldine base [2,13,14]. The emeraldine form is the most stable and conductive [2,13]. The PANI has many advantages, such as ease of synthesis, low cost, good environmental stability, and the ability to be electrically switched between its conductive and resistive states [15–19]. Unfortunately, its use in biological applications is limited by its low processibility, lack of flexibility and non-biodegradability, and has been noted to cause chronic inflammation once implanted [3,16,20]. Indeed, the conductive polymers maintenance in the body for a long time may cause chronic inflammation and requires surgical for removal, thereby introducing biodegradability to conductive polymers is mandatory [21]. Biodegradable synthetic polymers, such as polyesters, are now being utilized as promising materials for bone tissue engineering scaffolds [22–24]. In addition to their great mechanical properties, polyesters offer some advantages over other materials. For example, they can be fabricated into various shapes with desired pore architectures and morphologies. Among the aliphatic polyester family, poly(ϵ -caprolactone) (PCL) is one of the most excellent biocompatible and biodegradable polymers. It has outstanding processability because of its low melting point and good solubility in organic solvents [25]. The PCL dissolves in acetone, tetrahydrofuran, chloroform, methylene chloride, dimethylformamide (DMF), acetic acid, and formic acid [26–31]. The PCL is a semicrystalline linear hydrophobic polymer, FDA approved, and has a long history of safe use in human body. The electrospun PCL fibers mimic the identity of extra cellular matrix (ECM) in

living tissues; however, their poor hydrophilicity decreases the ability of cell adhesion, proliferation, and differentiation [32].

The success of a tissue engineering scaffold is associated with the following features: biocompatibility, biodegradability, hydrophilicity, suitable surface topography for efficient transmission of respiratory gases and waste, mechanical integrity, storage and release of active molecules, the ability to absorb and integrate in human body [33]. The selection of a suitable method for production of nanoscale scaffolds is a key factor in the success of tissue engineering. The scaffold coating is one of the most effective techniques for providing desirable scaffolds in particular applications. The coating of synthetic scaffolds with a natural polymer improves the cell adhesion and degradation rate [34]. Gelatin is a natural biopolymer derived from collagen which is biodegradable, biocompatible and has been widely used in the pharmaceutical and medical fields [34,35]. Therefore, gelatin can be coated on PCL nanofibers to obtain a scaffold with the desired cell adhesion and degradation properties [36]. The nanofibers fabricated with electrospinning technique are also used in the scaffold preparation for tissue engineering. Topology of three-dimensional (3D) nanostructure is similar to fibers in ECM proteins in the body. In fact, the nanotechnology has provided a possibility to produce the nanoscale microenvironments as in original ECM. In addition, the cells are sensitive to local nanoscale topographic pattern. Subsequent control of cellular function by nanoscale topographic guidance and engineered layers with different characteristics has been readily accepted [37,38].

In addition, the porous hydroxyapatite-gelatin composite scaffolds were fabricated for bone tissue engineering [39]. The synthesis and characterization of a laminated hydroxyapatite-gelatin nanocomposite scaffold with controlled pore structure was also represented for the bone applications [40]. Maleki et al. [41] reported a novel honey-based nanofibrous scaffold for wound dressing applications. A healing potential of mesenchymal was cultured on a collagen-based scaffold for skin regeneration [42]. Very recently, Sarvari et al. [43] applied an effective method for preparation of nanofibers using conducting polymer-functionalized reduced graphene oxide (rGO).

In the current work, we aimed to design the 3D nanostructured and conductive scaffolds with the appropriate mechanical and hydrophilic properties. For this purpose, first, the copolymer 2-hydroxyethylmethacrylate and N-isopropylacrylamide (P(HEMA-*b*-NIPAAm)) was successfully synthesized via reversible addition of fragmentation chain transfer (RAFT) polymerization. In the next step, P(HEMA-*b*-NIPAAm) reacted with ϵ -polycaprolactone through ring opening polymerization (ROP) to obtain P(HEMA-*b*-NIPAAm-*b*-CL) terpolymer. The electrospun nanofibers of terpolymers and PANI were prepared by electrospinning to reach the uniform fibers with diameters less than 100 nm for tissue engineering. The morphologies, electrical conductivities, biocompatibilities (adhesion and proliferation of osteoblast MG63 cells), mechanical properties and hydrophilicity of the nanofibers were investigated.

2. Experimental

2.1. Materials

The 2-hydroxyethyl methacrylate (HEMA) monomer was purchased from Merck (Darmstadt, Germany), dried over calcium hydride, vacuum-distilled, and then stored at $-20\text{ }^{\circ}\text{C}$ prior to use. The N-isopropylacrylamide (NIPAAm, 97%, Sigma-Aldrich, USA) was purified by recrystallization from *n*-hexane/toluene mixture (90/10 v/v) before use. The initiator of 2,2'-azobisisobutyronitrile (AIBN; Fluka, Switzerland) was recrystallized from ethanol at $50\text{ }^{\circ}\text{C}$ before use. The PCL having a number average molecular weight (M_n) of $70000\text{--}90000\text{ g mol}^{-1}$ was purchased from Merck. Caprolactone (CL, 99%) was purchased from Merck and distilled under reduced pressure over calcium hydride (CaH_2) prior to use. Tin(II) 2-ethylhexanoate ($\text{Sn}(\text{Oct})_2$) was prepared from Sigma-Aldrich (USA). Aniline monomer was purchased from Merck (Darmstadt, Germany) and distilled twice under reduced pressure before use. All other reagents were purchased from Merck and purified according to the standard methods.

2.2. Synthesis of 4-cyano-4-((thiobenzoyl)sulfanyl) pentanoic acid as a RAFT agent

The RAFT agent of 4-cyano-4-[(phenylcarbothiyl)sulfanyl] pentanoic acid was synthesized in our laboratory. Bis(thiobenzoyl) disulfide was prepared according to the reported

procedure by Le et al. [44]. The target compound of 4-cyano-4-((thiobenzoyl)sulfanyl) pentanoic acid was synthesized by heating the mixture of diphenyl dithioperoxy anhydride (1.62 g) and 4,4-azobis(4-cyanopentanoic acid) (1.62 g) in 60 mL ethyl acetate at $85\text{ }^{\circ}\text{C}$ for 18 h while purging with nitrogen. After eliminating the solvent by a rotary evaporator, the crude product was obtained and subjected to column chromatography by using a mixture of ethyl acetate and *n*-hexane with a ratio of 3:2 to yield an oily red compound (2.23 g, 69%) (Fig. 1(a)).

2.3. Synthesis of PHEMA via RAFT polymerization technique

A dry polymerization ampoule was charged with HEMA monomer (3.7 mL, 30.0 mmol), AIBN (5.0 mg, 0.03 mmol), RAFT agent (56.0 mg, 0.2 mmol), and dried N,N-dimethylformamide (DMF; 10 mL). The polymerization ampoule was degassed with several freeze-pump-thaw cycles, sealed off under vacuum, and placed in an oil bath at $70 \pm 3\text{ }^{\circ}\text{C}$ for 20 h. At the end of this time, the reaction was stopped by cooling of polymerization ampoule in ice/water bath. The reaction mixture was diluted with DMF (10 mL) and precipitated in cold diethyl ether (100 mL). The product was washed with diethyl ether several times, and dried under reduced pressure at room temperature [45]. Figure 1(b) represents the structure of synthesized PHEMA.

2.4. Synthesis of P(HEMA-*b*-NIPAAm)

The synthesized PHEMA was employed as a macro-RAFT agent for block copolymerization of NIPAAm monomer. In brief, a dry polymerization ampoule was charged with macro-RAFT agent (PHEMA, 1.0 g, 0.09 mmol), NIPAAm monomer (0.87 g, 7.7 mmol), AIBN (2.5 mg, 15 μmol) and DMF (10 mL). The resulted copolymer in this experiment was P(HEMA-*b*-NIPAAm). The polymerization ampoule was degassed with several freeze-pump-thaw cycles, sealed off under vacuum, and placed in an oil bath at $70 \pm 3\text{ }^{\circ}\text{C}$ for about 48 h. At the end, the ampoule was cooled in ice/water bath for quenching the reaction. The mixture was diluted with DMF (10 mL), and then precipitated in cold diethyl ether (100 mL). The product was filtrated and dried under reduced pressure at room temperature to reach a yellowish powder (Fig. 1(c)) [45].

2.5. Synthesis of P(HEMA-*b*-NIPAAm-*b*-CL) terpolymer

The terpolymers were prepared in a three-neck round bottle flask equipped with an inlet and outlet tube for nitrogen and thermometer. The CL monomer was fed to the reactor with a proper

amount of P(HEMA-*b*-NIPAAm) dissolved in DMF previously. The reaction mixture was agitated at 100 °C for 1 h to ensure that P(HEMA-*b*-NIPAAm) was completely dissolved in CL monomer. Sn(Oct)₂ (0.03 mol %) soluble in 2 mL toluene, was then added to the homogenous reaction mixture. The

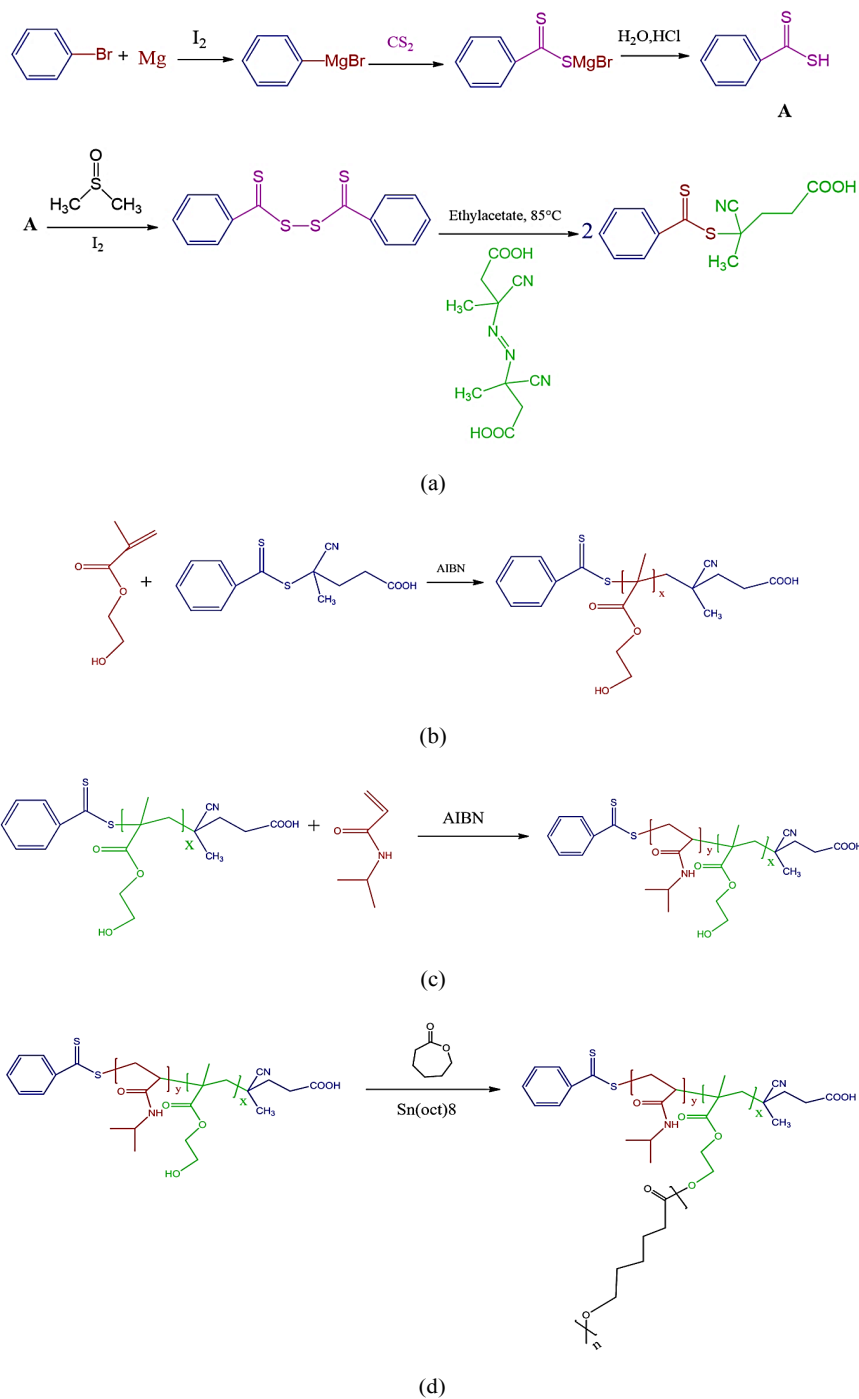


Fig. 1- Synthesis of (a) 4-cyano-4-(thiobenzoyl)sulfanyl pentanoic acid as a RAFT agent; (b) PHEMA; (c) P(HEMA-*b*-NIPAAm); (d) P(HEMA-*b*-NIPAAm-*b*-CL) terpolymer.

reaction was carried out at 140 °C for 18 h under nitrogen atmosphere. At the end of this time, the brown product was precipitated in diethylether and dried in vacuum at room temperature (Fig. 1(d)). The degree of polymerization (DP_n) and M_n were determined using ^1H NMR and gel permeation chromatography (GPC).

2.6. Electrospinning of P(HEMA-*b*-NIPAAm-*b*-CL) with PANI and PCL

The electrospinning apparatus was equipped with a high voltage power supply. First, P(HEMA-*b*-NIPAAm-*b*-CL) (3% w/v) and PANI (1% w/v) dissolved in dimethyl sulfoxide (DMSO) and high molecular weight PCL ($M_n = 70000\text{--}90000\text{ g mol}^{-1}$) dissolved in CHCl_3 at 5% w/v, then were stirred until the mixture became homogeneous. Blend solutions were prepared from P(HEMA-*b*-NIPAAm-*b*-CL):PANI:PCL with ratio of 65:25:10(v/v). P(HEMA-*b*-NIPAAm-*b*-CL)/PANI:PCL was added to a 10 mL syringe with a 23 Gauge hypodermic needle used as the nozzle. The flow rate of the polymer solution was controlled with a precision pump to maintain a steady flow from the capillary outlet. The experimental temperature was controlled at 25 °C. The solutions were injected at the rate of 0.3 mL/h, and the applied voltage was set to 23 kV. The static collector was wrapped with aluminum foil and located at a fixed working distance of 20 cm from the needle tip. After fiber deposition, the fiber mats were dried at room temperature until any solvent residue was completely removed.

2.7. Cell adhesion and proliferation

Nanofiber samples were sterilized under ultraviolet (UV) radiation for 30 min. The mouse osteoblast MG63 cells were used to investigate the cell adhesion and viability of the materials. The cells were rinsed three times with 0.1 M phosphate-buffered saline (PBS) by centrifugation at 1000 rpm for 5 min and cultured in cell culture flasks in a density of $2.0 \times 10^4/\text{cm}^2$ with RPMI 1640 medium (GIBCO) supplemented with 10% fetal calf serum (Gibco), $1.0 \times 10^5/\text{L}$ penicillin (Sigma), and 100 mg/L streptomycin (Sigma), in a humidified incubator at 37 °C and 5% CO_2 . The medium was changed every 2 days. After 3–5 days culture, the monolayer mouse osteoblast MG63 cells were removed from the cell culture flasks by trypsin (0.25%) treatment and rinsed three times with 0.1 M PBS by centrifugation at 1000 rpm for 5 min.

The obtained mouse osteoblast MG63 cells were resuspended in the medium to adjust cell density to 1.0×10^5 cells/well (in 1 mL of medium), then seeded on the nanofibers which were placed into 6-well plates (Costar) and tissue-culture-treated polystyrene (TCPS) (the empty 6-well plates) before being sterilized under UV radiation for 30 min and washed three times with PBS. Subsequently, 3 mL of medium was added into each well to prevent the cover slide from floating during cell seeding. The plates were incubated at 37 °C and 5% CO_2 for 3, 6, 9 and 24 h. The nanofibers were washed three times with PBS and fixed with 3% glutaraldehyde in PBS at room temperature for 30 min, washed with distilled water and dried in air. After some culture time, the cells were fixed with glutaraldehyde at room temperature and stained by DMSO solution with 2% FITC fluorescein (Sigma) for 10 min, then washed by PBS solution for three times. Cell attachment and proliferation were observed under the reverse microscope (TE2000U, Nikon). The fluorescence pictures were taken by Digital Camera DXM1200F (Nikon) and analyzed with "NIH Image J" software (>20 per sample). The data presented are the mean (standard deviation (SD)). Independent and replicated experiments were used to analyze the statistical variability of the data, with $p < 0.05$ being statistically significant.

2.8. MTT Experiment

The cytotoxicity of nanofibers was assayed using 3-(4,5-dimethylthiazol-2-yl)-2,5-diphenyltetrazolium bromide (MTT). First, samples were put into RPMI 1640 medium (Gibco) supplemented with 10% fetal calf serum (Gibco) for 48 h at 37 °C to get their extract liquid with the concentrations of 100, 50, 25, 12.5, 6.25, 3.125 and 1.5625 mg/mL. The MG63 cells were seeded in 96-well plates at a density of 12000 cells per well and medium changed after 24 h incubation. Various concentrations of extract liquid were then added to the wells. After incubating for 24 h, 20 μL of MTT nal concentration of 0.5 mg/mL MTT. The plate was then incubated at 37 °C in 5% CO_2 for 4 h. The medium was removed and 200 μL of DMSO was added to dissolve the formazan crystals. The optical density (OD) was measured at 492 nm by a microplate reader (Multiskan MK3, Thermo USA). The untreated cells were taken as control with 100% viability. The relative cell viability (%) compared to control cells was calculated by [abs]

sample/[abs]control \times 100.

2.9. Characterization

Fourier transform infrared (FT-IR) spectra of the samples were collected at room temperature on a Shimadzu 8101M FT-IR (Shimadzu, Kyoto, Japan) in the frequency range of 4000 to 400 cm^{-1} with an attenuated total reflection facility. The nuclear magnetic resonance (^1H NMR) spectra of the samples were recorded at 25 $^\circ\text{C}$ using an ^1H NMR (400 MHz) Bruker spectrometer (Bruker, Ettlingen, Germany). The sample for ^1H NMR spectroscopy was prepared by dissolving about 10 mg in 1 mL of deuterated dimethylsulfoxide (DMSO-d_6) or deuterated chloroform (CDCl_3), and chemical shifts were reported in parts per million (ppm) units with tetramethylsilane (TMS) as internal standard. The field emission scanning electron microscope (FESEM) type 1430 VP (LEO Electron Microscopy Ltd, Cambridge, UK) was applied to determine the morphologies of samples. The average molecular weight of terpolymer was determined by gel permeation chromatograph with Agilent, PLgel Mixed-C, 5 μm , 300 \times 7.5 mm columns (GPC Agilent 1100) and refractometer index detector at 30 $^\circ\text{C}$. DMF was utilized as an eluent at a flow rate of 1 mL/min and the system was calibrated with polystyrene standard. Electrochemical experiments were conducted using Auto-Lab PGSTA T302N. The electrochemical cell contained five openings, three of them were used for the electrodes (working, counter, and reference), and two for argon bubbling in the solutions during all experiments. The conductivities of the synthesized samples were determined using a four-probe technique (Azar Electrode, Urmia, Iran) at room temperature. The tensile strength and strain

to break were detected with a Zwick tensile testing machine (Z 010, Zwick/Roell, Ulm, Germany). The wettability of the electrospun nanofibers were investigated by drop water contact angle measurement employing an OCA 20 plus contact angle meter system (Data Physics Instruments GmbH, Filderstadt, Germany). The droplet size was 5 μL and at least five samples were used for each test.

3. Results and discussion

The electrical stimulation can modify the cellular activities subsuming the cell migration [46], cell adhesion [47], DNA synthesis [48,49] and protein secretion [50]. This makes electrical stimulation potentially highly significant in tissue engineering, because regulating these cellular activities in an artificial scaffold is important in controlling the regeneration of damaged tissues. Hence, an electrically conductive scaffold could be used either in vitro or in vivo to host cells that would be subsequently regulated by the electrical current or field applied through the scaffold. However, to use this rule in tissue engineering, a new type of biomaterial is required. This novel material should be electrically conductive, biocompatible, and ideally biodegradable. Furthermore, because the regeneration of tissues such as the sciatic nerve in rat requires 1–2 months or even longer, the ability to sustain a long-term electrical stimulation or the electrical stability of such conductive material must also be investigated [51]. In this paper, P(HEMA-*b*-NIPAAm-*b*-CL) terpolymer blended with PANI was an appropriate candidate for preparation of scaffold because of conductivity, biodegradability, hydrophilicity and mechanical properties.

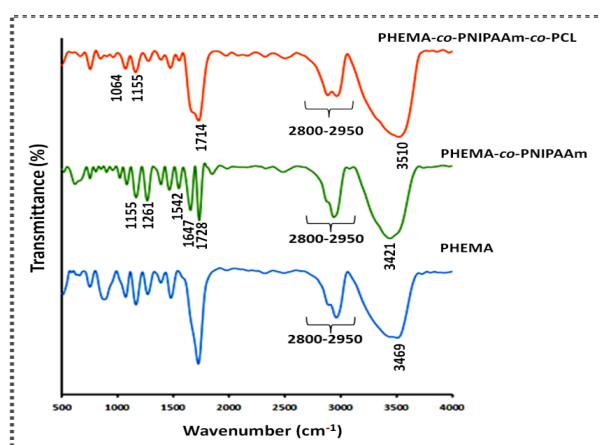


Fig. 2- FT-IR spectra of PHEMA, P(HEMA-*b*-NIPAAm), and P(HEMA-*b*-NIPAAm-*b*-CL).

3.1. Characterization of synthesized P(HEMA-*b*-NIPAAm-*b*-CL)

3.1.1. FT-IR spectra of P(HEMA-*b*-NIPAAm-*b*-CL)

FT-IR spectra of P(HEMA-*b*-NIPAAm-*b*-CL), P(HEMA-*b*-NIPAAm), and PHEMA are displayed in Fig. 2. The most important bands in FT-IR spectrum of PHEMA as followed: aliphatic C-H stretching vibrations at 2800–2950 cm^{-1} , the stretching vibration of carbonyl group at 1718 cm^{-1} , C-H bending vibration at 1471 cm^{-1} , the stretching vibration of C-O group at 1371 cm^{-1} , C-O-C stretching vibration at 1155 cm^{-1} , and the stretching vibration of hydroxyl group as a strong broad band centered at 3438 cm^{-1} . FT-IR spectra of P(HEMA-*b*-NIPAAm) diblock copolymers depicted the typical bands corresponding to both PHEMA and PNIPAAm segments. The main absorption bands in this sample were the stretching vibrations of carbonyl groups of PHEMA and PNIPAAm at 1730 and 1652 cm^{-1} , respectively. The absorption bands due to -NH secondary amid and hydroxyl groups were overlapped and led to a very strong and broad band centered at 3456 cm^{-1} , aliphatic-CH stretching vibration bands around 2800 to 2950 cm^{-1} , and -CH bending vibrations at 1458 and 1392 cm^{-1} [45]. Moreover, FT-IR spectra of P(HEMA-*b*-NIPAAm-*b*-CL) terpolymers demonstrated the typical bands corresponding to both PHEMA, PNIPAAm, and PCL segments. The stretching vibration of carbonyl group at 1714 cm^{-1} verified the synthesis of terpolymer.

3.1.2. ^1H NMR spectroscopy

^1H NMR spectra of PHEMA (Fig. 3(a)) demonstrated the chemical shifts at 0.75–0.95 and 1.75–2.05 ppm associated with the methyl and methylene protons of PHEMA backbone, respectively. The chemical shifts at 3.55 and 3.85 ppm were related to -CH₂OH and -CH₂ protons, respectively. The chemical shift at 4.80 ppm was correlated with the hydroxyl group of PHEMA. In addition, the chemical shift at 7.95 ppm was corresponded to the aromatic protons of RAFT agent. As illustrated in ^1H NMR spectra of Fig. 3(b) for P(HEMA-*b*-NIPAAm) copolymers, almost all chemical shifts of PNIPAAm segment were overlapped with the chemical shifts of PHEMA. The most significant change in this spectrum was the appearance of new chemical shift at 1.15 ppm related to the methylene (-CH-CO) group of PNIPAAm backbone [45]. The successful synthesis

of P(HEMA-*b*-NIPAAm-*b*-CL) terpolymers was verified by the appearances of new chemical shifts (b, c, e, h, h' and k) that were attributed to PCL. The peaks of b, c, and e were detected at 1.30, 1.54, and 2.27 ppm, respectively. The peak of methylene protons (h) appeared at 3.97 ppm. Furthermore, the peak of the protons of terminal methylene (h') was observed at 3.82 ppm. The peak at 4.17 ppm indicated that the PCL was terminated by the hydroxyl groups (Fig. 3(c)).

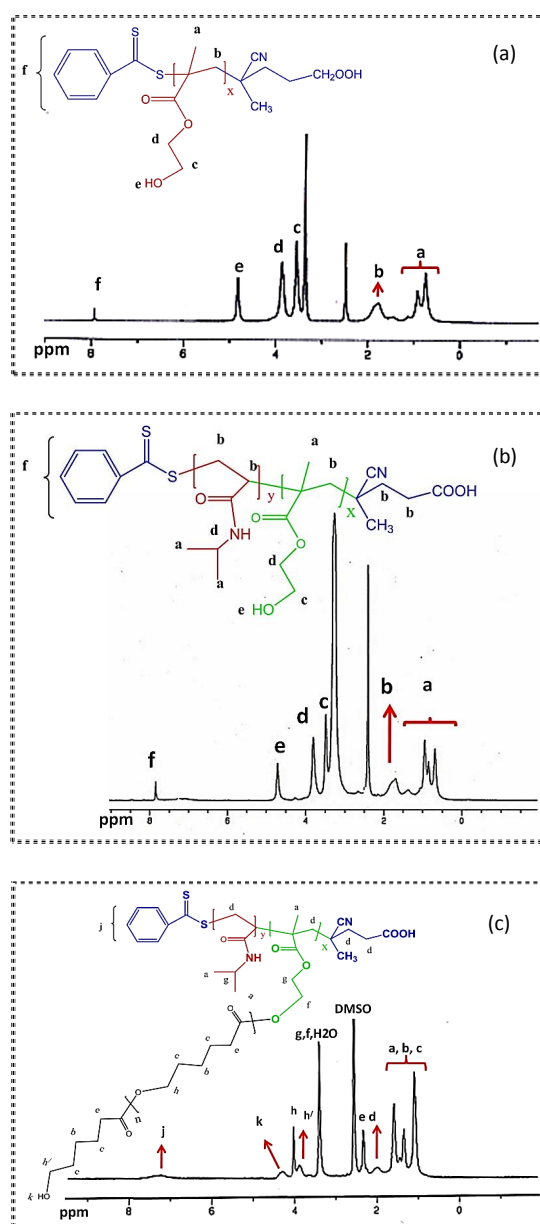


Fig. 3- ^1H NMR spectra of PHEMA (a), P(HEMA-*b*-NIPAAm) (b), and P(HEMA-*b*-NIPAAm-*b*-CL) (c).

3.2. GPC analysis for verification of molecular weights

The GPC chromatograms of PHEMA, P(HEMA-*b*-NIPAAm), and P(HEMA-*b*-NIPAAm-*b*-CL) samples are shown in Fig. 4. The polydispersity indices (PDIs) of PHEMA ($M_n = 11201$ g/mol and PDI = 1.13), P(HEMA-*b*-NIPAAm) ($M_n = 14820$ g/mol and PDI = 1.17), and P(HEMA-*b*-NIPAAm-*b*-CL) ($M_n = 32676$ g/mol and PDI = 1.20) synthesized via RAFT polymerization were relatively low. The results demonstrated a well-controlled RAFT polymerization. As reported in Table 1, a high consistency was detected between GPC and ¹HNMR analyses.

3.3. Electroactivity characteristics

The PANI has been utilized in the novel intelligent scaffolds for cardiac and neuronal tissue engineering applications [52–57]. The basic idea was that the cell proliferation, assembly, and particularly, differentiation might be influenced, directed or even controlled by electrical or electrochemical stimulation applied through the electroactive scaffold materials. The electrical

charges play an important role in stimulating either proliferation or differentiation of various cell types. The electroactive polymers provide potentially interesting surfaces for cell culture in which their properties (e.g., surface charge, wettability, and conformational and dimensional changes) can be altered reversibly by chemical or electrochemical oxidation or reduction [58,59]. Recent studies have demonstrated that the PANI and its derivatives can function as biocompatible substrates, upon which both H9c2 cardiac myoblasts and PC12 pheochromocytoma cells were found to adhere, grow and/or differentiate well [54–57,60]. Cyclic voltammetry is a powerful electrochemical equipment to reach the information about electrochemical behaviors and interconversion of oxidation states of PANI. The peaks in the cyclic voltammograms (CV), which are ascribed to the electrochemical responses of PANI, represent an information about the charge injected during interconversion of any two oxidation states of PANI. The effect of different anions in the supporting electrolyte or polymerization medium on the conductivity or morphology of PANI can also be

Table 1- The characteristics of synthesized polymers

Sample	$M_n^{a(GPC)}$	$M_n^{b(HNMR)}$	PDI ^a
PHEMA	11201	10736	1.13
P(HEMA- <i>b</i> -NIPAAm)	14820	14665	1.17
P(HEMA- <i>b</i> -NIPAAm- <i>b</i> -CL)	32676	31938	1.20

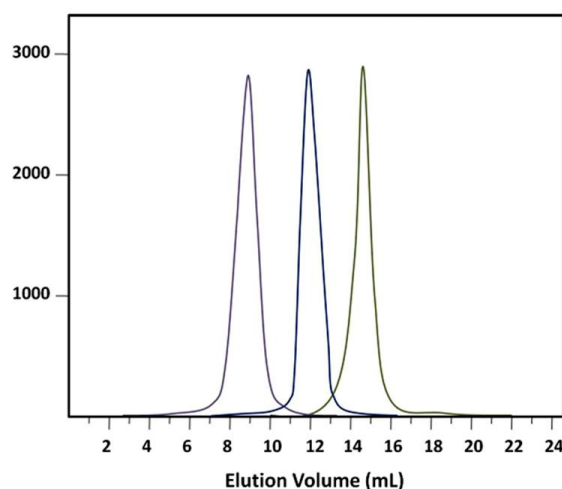


Fig. 4- GPC traces of PHEMA (green), P(HEMA-*b*-NIPAAm) (dark blue), and P(HEMA-*b*-NIPAAm-*b*-CL) (purple) in DMF as eluent.

studied using cyclic voltammetry [61]. The CVs obtained from the films of electrochemically grown PANI onto P(HEMA-*b*-NIPAAm-*b*-CL)/PANI prepared on glassy carbon (GC) microelectrode in the constant scan rate of 25 mV s^{-1} for 10 cycles in the sulfuric acid (1 mol L^{-1}) between -0.20 and $+1.20 \text{ V}$ versus the reference electrode are depicted in Fig. 5(a). Herein, two anodic peaks at approximately 0.40 and 0.60 V were detected versus the reference electrode. The CVs of electrochemically growth of PANI onto P(HEMA-*b*-NIPAAm-*b*-CL)/PANI film in the range of 10 to 100 mV s^{-1} scan rates in the sulfuric acid between -0.20 and $+1.20 \text{ V}$ versus the reference electrode exhibited two anodic peaks which shifted in the direction of higher potentials with increasing the scan rate. The final anodic peaks at the highest scan rate reached in 0.65 and 0.80 V versus the reference electrode (Fig. 5(b)). Therefore, the electrochemical oxidation/reduction of the casted films was chemically reversible. The CVs of chemically synthesized P(HEMA-*b*-NIPAAm-*b*-CL)/PANI in the constant rate of 25 mV s^{-1} was depicted in Fig. 5(c). The CVs of P(HEMA-*b*-NIPAAm-*b*-CL)/PANI film exhibited two anodic

peaks at approximately 0.3 and 0.65 V versus the reference electrode. The effect of potential scanning rate (V) on the peak currents for chemically synthesized P(HEMA-*b*-NIPAAm-*b*-CL)/PANI was investigated under cyclic voltammetric conditions in the range of 10 to 80 mV s^{-1} scan rates in sulfuric acid (1 mol L^{-1}) between -0.20 and $+1.20 \text{ V}$ versus the reference electrode. As seen in Fig. 5(d), the CVs of P(HEMA-*b*-NIPAAm-*b*-CL)/PANI film demonstrated two anodic peaks versus the reference electrode. The electrochemical oxidation/reduction of the casted films was chemically reversible. These analyses confirmed the considerable potential of prepared electroactive copolymer for the biomedical applications.

3.4. Morphology, hydrophilicity, mechanical and biodegradability properties of electrospun nanofibers

Fig. 6(a) illustrates FESEM image of the blended nanofibers of P(HEMA-*b*-NIPAAm-*b*-CL)/PANI. FESEM images represented a uniform morphology and also a 3D interconnected pore structure having the diameters ranged in 60 – 130 nm (Fig.

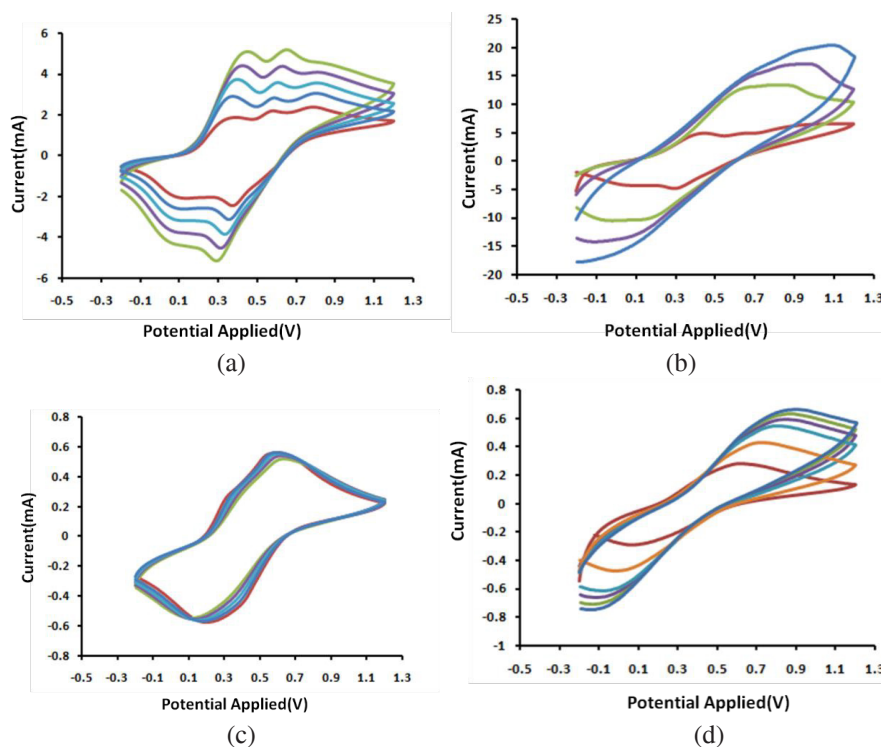


Fig. 5- Cyclic voltammetry curves of electrochemically growth of PANI onto P(HEMA-*b*-NIPAAm-*b*-CL) in 25 mV s^{-1} scan rate (a); electrochemically growth of PANI onto P(HEMA-*b*-NIPAAm-*b*-CL) in 10 – 60 mV s^{-1} scan rate (b); chemically synthesized P(HEMA-*b*-NIPAAm-*b*-CL) in 25 mV s^{-1} scan rate (c); chemically synthesized P(HEMA-*b*-NIPAAm-*b*-CL) in 10 – 80 mV s^{-1} scan rate (d) in the aqueous solution of sulfuric acid (1 mol L^{-1}) between -0.20 and $+1.20 \text{ V}$.

6(a)). In addition, the contact angle reflected the hydrophilicity of scaffolds, which could further influence the extent of protein adsorption and cell attachment [62]. The surface hydrophilicity of electrospun scaffolds was measured by water contact angle test. The contact angle was $49 \pm 5^\circ$. The photograph of water drop on P(HEMA-*b*-NIPAAm-*b*-CL)/PANI via a standard method [63] is reported in the inset panel of Fig. 6(a). An evidence for the in vitro degradability of P(HEMA-*b*-NIPAAm-*b*-CL) nanofibers was obtained through evaluating the morphological changes after soaking the nanofibers in PBS at 37°C. Fig. 6(b) displays FESEM image of the sample after 30 days soaking with a swollen and degraded status.

The biological scaffolds should have ability to impart specific mechanical effects that improve

the cell behavior. The select of type and material of scaffold is the most important part of work. A scaffold not only allows the connections of cells, but also causes the cell migration, transport and transfer of biochemical factors, the release of nutrients, waste and material of the cells. To this end, a scaffold must have a series of structural features like good mechanical properties. The intensity of mechanical resistance of a scaffold should be tailored to the target tissue or site of implantation [64]. The mechanical parameters of P(HEMA-*b*-NIPAAm-*b*-CL)/PANI electrospun nanofibers are shown in Fig. 7. The sample exhibited a linear elastic behavior before failure. Based on obtained results, Young's modulus, tensile strength, and elongation at break were 955 ± 50.5 MPa, 32 ± 4.8 MPa, and

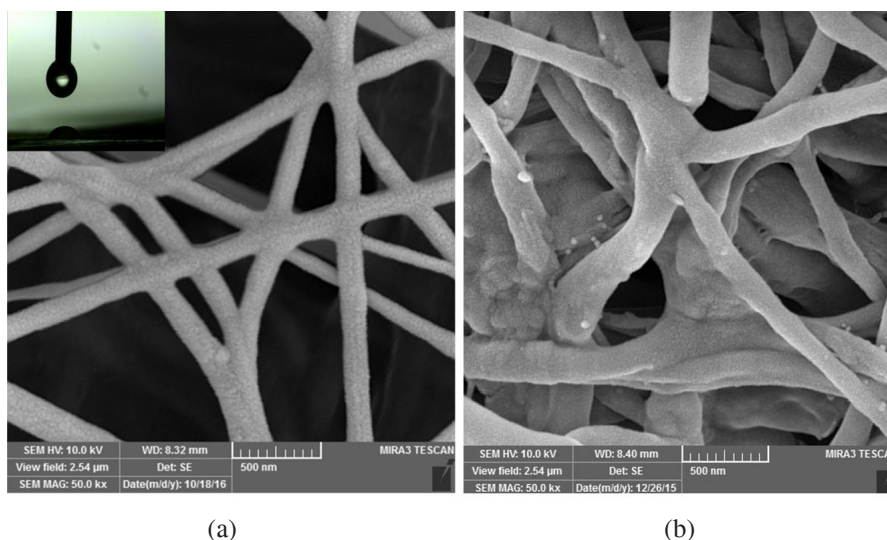


Fig. 6- FESEM images of (a) P(HEMA-*b*-NIPAAm-*b*-CL)/PANI nanofibers and photograph of water drop on them in the inset panel; (b) P(HEMA-*b*-NIPAAm-*b*-CL)/PANI nanofibers after 30 days soaking in PBS.

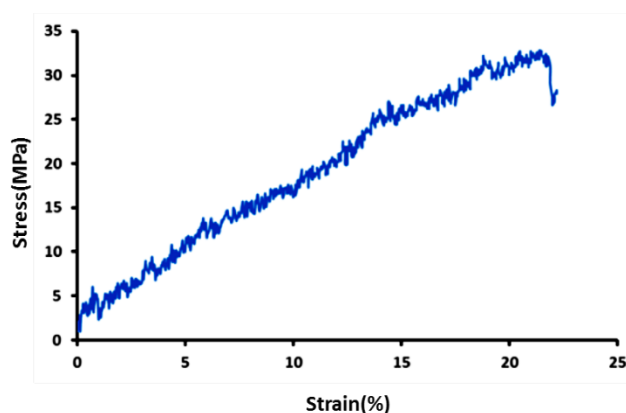


Fig. 7- Stress-strain curves of P(HEMA-*b*-NIPAAm-*b*-CL)/PANI electrospun nanofibers.

$21 \pm 3.4\%$, respectively. The stress-strain curve of electrospun scaffold was recorded from the load deformation curve at a deforming speed of 5 mm/min.

3.5. Electrical conductivity measurement

Many cell types including the neurons, osteoblasts, and fibroblasts respond to the electrical currents [65–70], thereby the conductive scaffolds could play a role in tissue engineering. In fact, the bioelectricity in the human body participates in maintaining normal biological functions like signaling of the nervous system, muscle contraction and wound healing [71]. The presence of a steady weak direct current (DC) electrical field in some biological systems affects cellular activities such as cell division, differentiation, migration and the extension of motile processes [72]. Conducting polymers such as PANI demonstrate the excellent cellular activities through electrical stimulation, leading to application of their derivatives as pro-regenerative tissue scaffolds [73,74]. The electrical conductivities of synthesized sample and electrospun nanofibers were measured at room temperature using a standard four-probe technique. The experiments were repeated five times for each sample to evaluate the sample accuracy. Electrical conductivity (σ) was then calculated according to the literature [21]. The electrical conductivities

of PANI, P(HEMA-*b*-NIPAAm-*b*-CL)/PANI, and electrospun nanofibers were 0.78, 0.66, and 0.03, respectively. The P(HEMA-*b*-NIPAAm-*b*-CL)/PANI possessed a slightly lower electrical conductivity compared to PANI. However, the lower electrical conductivity levels in these samples can be improved at the price of solubility, processability, and biocompatibility. In addition, the conductivity in the semiconductor range ($\sim 10^{-5} \text{ S cm}^{-1}$) might be sufficient to conduct micro-current for stimulating neuronal cell proliferation, and possibly differentiation because the micro-current intensity is very low in human body [21].

3.6. Biocompatibility

3.6.1. Cytotoxic effect of the electrospun nanofibers

The potential cytotoxic effect of P(HEMA-*b*-NIPAAm-*b*-CL)/PCL/PANI electrospun nanofiber on mouse osteoblast MG63 cells were investigated by MTT assay. The results showed that the prepared electrospun nanofibers were not able to induce cytotoxicity in mouse osteoblast MG63 cells (Fig. 8).

3.6.2. Cell growth assay and morphology study

The biocompatibility of the tissue engineering scaffolds is a vital concern because of its influence on the cell attachment, proliferation, migration, differentiation and neo-tissue formation. The cell growth performance of P(HEMA-*b*-NIPAAm-*b*-CL)/PCL/PANI electrospun nanofiber surfaces were evaluated at the initial seeding densities of $1 \times 10^5 \text{ cells cm}^{-2}$ using mouse osteoblast MG63 cells as shown in Fig. 9(a). The results represented that in the case of P(HEMA-*b*-NIPAAm-*b*-CL)/PCL/PANI nanofibers, the fibroblast cells were expanded 8 ± 0.5 factor, and reached $8 \pm 0.5 \times 10^5 \text{ cells cm}^{-2}$ at the end of the cell culture period.

The morphology of osteoblast cultured on the scaffold was studied by FESEM after 7 days in culture. Fig. 9(b) depicts the morphology of osteoblast cells cultured in the interior of the scaffold. The osteoblast cells tightly adhered to P(HEMA-*b*-NIPAAm-*b*-CL)/PANI hollow fibers and formed integrated cell-fiber constructs. The scaffold structure ensured that the cells could easily migrate into the interior part, thus a 3D culture of osteoblast could be achieved. The cells in these constructs exhibited wide cell-cell contact which is helpful for the maintenance of cell activity and function, and also promotes the

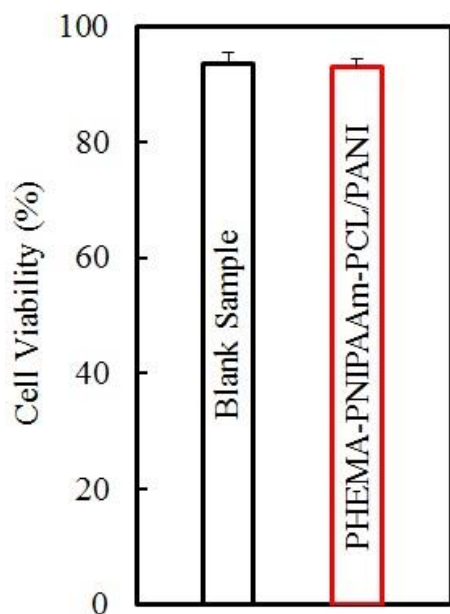
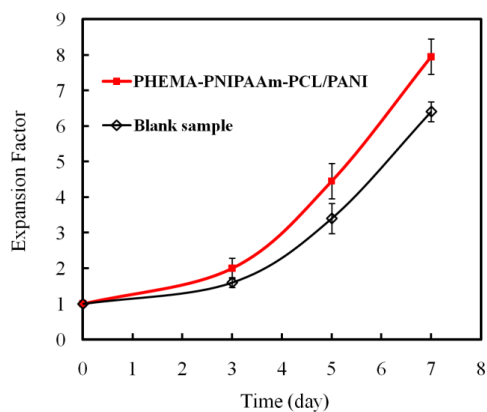


Fig. 8- In vitro cytotoxicity effect of P(HEMA-*b*-NIPAAm-*b*-CL)/PCL/PANI electrospun nanofibers on mouse osteoblast MG63 cells.

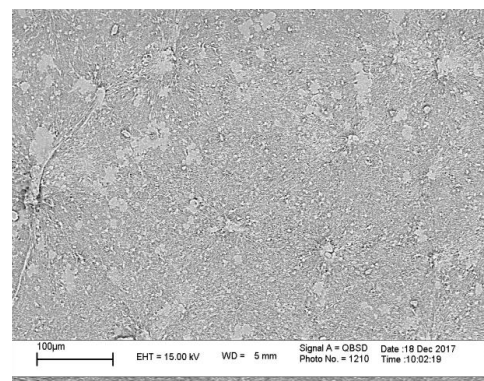
cell proliferation [75]. The novel 3D scaffold was capable of providing an interconnected porous structure and large surface area for osteoblast adhesion and proliferation. The alizarin red staining, an anthraquinone dye, has been widely used to evaluate calcium deposits in cell culture. The alizarin red and alkaline phosphatase (ALP) enzyme staining were used to evaluate the cell activities. The alizarin red staining is quite versatile because the dye can be extracted from the stained monolayer of cells and readily assayed. The staining of alizarin red activity was performed according to the standard instructions. The activity of cells was illustrated in Fig. 10 for P(HEMA-*b*-NIPAAm-*b*-CL)/PCL/PANI nanofibers. As shown in Fig. 10, the cell activity was suitable in contact with the nanofibers.

4. Conclusions

The novel 3D scaffolds were designed based on P(HEMA-*b*-NIPAAm-*b*-CL) blend with PANI. The electroactivity, mechanical, and hydrophilicity studies demonstrated that the electrospun scaffolds could be appropriate for tissue engineering. The electrospun nanofibers can provide suitable nano-environments for cell adhesion, migration, proliferation and differentiation. In this regard, P(HEMA-*b*-NIPAAm-*b*-CL) terpolymers were synthesized via RAFT and ROP methods. The terpolymers blended with PANI had a suitable electroactivity which improved the adhesion, growth, and proliferation of cells. The hydrophilicity of the electrospun nanofibers was significantly increased by P(HEMA-*b*-NIPAAm) segments, as confirmed by the contact angle measurements. Moreover, P(HEMA-*b*-



(a)



(b)

Fig. 9- Mouse osteoblast MG63 cells growth performance (a) and FESEM image of cells (b) on P(HEMA-*b*-NIPAAm-*b*-CL)/PCL/PANI electrospun nanofibers.

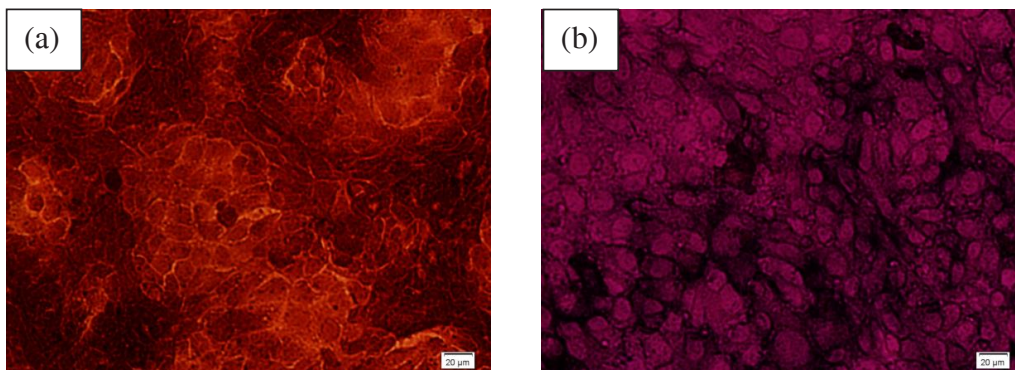


Fig. 10- P(HEMA-*b*-NIPAAm-*b*-CL)/PCL/PANI nanofiber activity with (a) alizarin red and (b) ALP tests.

NIPAAm-*b*-CL) terpolymers exhibited good solubility and mechanical properties. In vitro cell experiments demonstrated that the fabricated scaffolds were biocompatible with improved adhesion, proliferation and osteoblast cell growth characteristics. The P(HEMA-*b*-NIPAAm-*b*-CL)/PANI samples are good candidates for the electroactive polymers used in the biomedical field.

Acknowledgment

The authors express their gratitude to the Payame Noor University as well as Stem Cell and Tissue Engineering Research Laboratory at Sahand University of Technology.

References

- Lakard, B., et al., Effect of ultrasounds on the electrochemical synthesis of polypyrrole, application to the adhesion and growth of biological cells. *Bioelectrochemistry*, 2009. 75(2): p. 148-157.
- Ghasemi-Mobarakeh, L., et al., Application of conductive polymers, scaffolds and electrical stimulation for nerve tissue engineering. *Journal of Tissue Engineering and Regenerative Medicine*, 2011. 5(4): p. e17-e35.
- Huang, L., et al., Synthesis of Biodegradable and Electroactive Multiblock Polylactide and Aniline Pentamer Copolymer for Tissue Engineering Applications. *Biomacromolecules*, 2008. 9(3): p. 850-858.
- Rivers, T.J., T.W. Hudson, and C.E. Schmidt, Synthesis of a Novel, Biodegradable Electrically Conducting Polymer for Biomedical Applications. *Advanced Functional Materials*, 2002. 12(1): p. 33.
- Kotwal, A., Electrical stimulation alters protein adsorption and nerve cell interactions with electrically conducting biomaterials. *Biomaterials*, 2001. 22(10): p. 1055-1064.
- Lee, J.Y., et al., Polypyrrole-coated electrospun PLGA nanofibers for neural tissue applications. *Biomaterials*, 2009. 30(26): p. 4325-4335.
- Wallace, G.G., M. Smyth, and H. Zhao, Conducting electroactive polymer-based biosensors. *TrAC Trends in Analytical Chemistry*, 1999. 18(4): p. 245-251.
- Kim, D.H., et al., Effect of Immobilized Nerve Growth Factor on Conductive Polymers: Electrical Properties and Cellular Response. *Advanced Functional Materials*, 2007. 17(1): p. 79-86.
- Garner, B., et al., Polypyrrole-heparin composites as stimulus-responsive substrates for endothelial cell growth. *Journal of Biomedical Materials Research*, 1999. 44(2): p. 121-129.
- Aoki, T., et al., Secretory function of adrenal chromaffin cells cultured on polypyrrole films. *Biomaterials*, 1996. 17(20): p. 1971-1974.
- Guiseppi-Elie, A., Electroconductive hydrogels: Synthesis, characterization and biomedical applications. *Biomaterials*, 2010. 31(10): p. 2701-2716.
- Balint, R., N.J. Cassidy, and S.H. Cartmell, Conductive polymers: Towards a smart biomaterial for tissue engineering. *Acta Biomaterialia*, 2014. 10(6): p. 2341-2353.
- Zhou, D.D., et al., Conducting Polymers in Neural Stimulation Applications, in *Implantable Neural Prostheses 2*. 2009, Springer New York. p. 217-252.
- Blinova, N.V., et al., Control of polyaniline conductivity and contact angles by partial protonation. *Polymer International*, 2008. 57(1): p. 66-69.
- Cullen, D.K., et al., Developing a tissue-engineered neural-electrical relay using encapsulated neuronal constructs on conducting polymer fibers. *Journal of Neural Engineering*, 2008. 5(4): p. 374-384.
- Borriello, A., et al., Optimizing PANi doped electroactive substrates as patches for the regeneration of cardiac muscle. *Journal of Materials Science: Materials in Medicine*, 2011. 22(4): p. 1053-1062.
- Guo, Y., et al., Electroactive Oligoaniline-Containing Self-Assembled Monolayers for Tissue Engineering Applications†. *Biomacromolecules*, 2007. 8(10): p. 3025-3034.
- Prabhakaran, M.P., et al., Electrospun conducting polymer nanofibers and electrical stimulation of nerve stem cells. *Journal of Bioscience and Bioengineering*, 2011. 112(5): p. 501-507.
- Yu, Q.-Z., et al., Morphology and conductivity of polyaniline sub-micron fibers prepared by electrospinning. *Materials Science and Engineering: B*, 2008. 150(1): p. 70-76.
- Zhang, Q.-S., et al., Synthesis of a novel biodegradable and electroactive polyphosphazene for biomedical application. *Biomedical Materials*, 2009. 4(3): p. 035008.
- Sarvari, R., et al., Novel three-dimensional, conducting, biocompatible, porous, and elastic polyaniline-based scaffolds for regenerative therapies. *RSC Advances*, 2016. 6(23): p. 19437-19451.
- Bocaccini, A.R. and J.E. Gough, *Tissue engineering using ceramics and polymers*. 2007, Woodhead Publishing Limited.
- Hollander, A.P. and P.V. Hatton, *Biopolymer Methods in Tissue Engineering*. 2003, Humana Press.
- Shadjou, N. and M. Hasanzadeh, Bone tissue engineering using silica-based mesoporous nanobiomaterials:Recent progress. *Materials Science and Engineering: C*, 2015. 55: p. 401-409.
- Woodruff, M.A. and D.W. Hutmacher, The return of a forgotten polymer—Polycaprolactone in the 21st century. *Progress in Polymer Science*, 2010. 35(10): p. 1217-1256.
- Di Pasquale, N., et al., Solvent Structuring and Its Effect on the Polymer Structure and Processability: The Case of Water-Acetone Poly-ε-caprolactone Mixtures. *The Journal of Physical Chemistry B*, 2014. 118(46): p. 13258-13267.
- Yang, Q., et al., Preparation of Polycaprolactone Tissue Engineering Scaffolds by Improved Solvent Casting/Particulate Leaching Method. *Journal of Macromolecular Science, Part B*, 2006. 45(6): p. 1171-1181.
- Cannillo, V., et al., Production of Bioglass® 45S5 – Polycaprolactone composite scaffolds via salt-leaching. *Composite Structures*, 2010. 92(8): p. 1823-1832.
- Reignier, J. and M.A. Huneault, Preparation of interconnected poly(ε-caprolactone) porous scaffolds by a combination of polymer and salt particulate leaching. *Polymer*, 2006. 47(13): p. 4703-4717.
- Van der Schueren, L., et al., Polycaprolactone/chitosan blend nanofibres electrospun from an acetic acid/formic acid solvent system. *Carbohydrate Polymers*, 2012. 88(4): p. 1221-1226.
- Taherkhani, S. and F. Moztarzadeh, Fabrication of a poly(ε-caprolactone)/starch nanocomposite scaffold with a solvent-casting/salt-leaching technique for bone tissue engineering applications. *Journal of Applied Polymer Science*, 2016. 133(23).
- Reed, C.R., et al., Composite Tissue Engineering on Polycaprolactone Nanofiber Scaffolds. *Annals of Plastic Surgery*, 2009. 62(5): p. 505-512.
- Jha, B.S., et al., Two pole air gap electrospinning: Fabrication of highly aligned, three-dimensional scaffolds for nerve reconstruction. *Acta Biomaterialia*, 2011. 7(1): p. 203-215.
- Ghasemi-Mobarakeh, L., et al., Electrospun poly(ε-caprolactone)/gelatin nanofibrous scaffolds for nerve tissue engineering. *Biomaterials*, 2008. 29(34): p. 4532-4539.
- Lim, Y.C., et al., Micropatterning and characterization of electrospun poly(ε-caprolactone)/gelatin nanofiber tissue scaffolds by femtosecond laser ablation for tissue engineering applications. *Biotechnology and Bioengineering*, 2010. 108(1): p. 116-126.
- Safaeijavan R, Soleimani M, Divsalar A, Eidi A, Ardeshiryajimi A. Biological behavior study of gelatin coated PCL nanofibrous electrospun scaffolds using fibroblasts. *Journal of Paramedical Sciences (JPS) Winter*. 2014;5(1):2008-4978.
- Cunha, C., S. Panseri, and S. Antonini, Emerging

- nanotechnology approaches in tissue engineering for peripheral nerve regeneration. *Nanomedicine: Nanotechnology, Biology and Medicine*, 2011. 7(1): p. 50-59.
38. Atyabi, S.M., et al., Cell Attachment and Viability Study of PCL Nano-fiber Modified by Cold Atmospheric Plasma. *Cell Biochemistry and Biophysics*, 2015. 74(2): p. 181-190.
39. Kazemzadeh Narbat M, Orang F, Solati Hashtjin M, Goudarzi A. Fabrication of porous hydroxyapatite-gelatin composite scaffolds for bone tissue engineering. *Iranian Biomedical Journal*. 2006,10(4):215-23.
40. Azami, M., A. Samadikuchaksaraei, and S.A. Poursamar, Synthesis and Characterization of a Laminated Hydroxyapatite/Gelatin Nanocomposite Scaffold with Controlled Pore Structure for Bone Tissue Engineering. *The International Journal of Artificial Organs*, 2010. 33(2): p. 86-95.
41. Maleki, H., et al., The influence of process parameters on the properties of electrospun PLLA yarns studied by the response surface methodology. *Journal of Applied Polymer Science*, 2014. 132(5): p. n/a-n/a.
42. Shokrgozar MA, Fattahi M, Bonakdar S, Kashani IR, Majidi M, Haghighipour N, Bayati V, Sanati H, Saeedi SN. Healing potential of mesenchymal stem cells cultured on a collagen-based scaffold for skin regeneration. *Iranian biomedical journal*. 2012 Apr;16(2):68.
43. Sarvari, R., et al., Composite electrospun nanofibers of reduced graphene oxide grafted with poly(3-dodecylthiophene) and poly(3-thiophene ethanol) and blended with polycaprolactone. *Journal of Biomaterials Science, Polymer Edition*, 2017. 28(15): p. 1740-1761.
44. Le TP, Moad G, Rizzardo E, Thang SH. PCT Int. Appl. WO 9801478 A1 980115. InChem. Abstr 1998 (Vol. 128, p. 115390).
45. Davaran, S., et al., Novel dual stimuli-responsive ABC triblock copolymer: RAFT synthesis, "schizophrenic" micellization, and its performance as an anticancer drug delivery nanosystem. *Journal of Colloid and Interface Science*, 2017. 488: p. 282-293.
46. Li, X. and J. Kolega, Effects of Direct Current Electric Fields on Cell Migration and Actin Filament Distribution in Bovine Vascular Endothelial Cells. *Journal of Vascular Research*, 2002. 39(5): p. 391-404.
47. Pullar, C.E., R.R. Isseroff, and R. Nuccitelli, Cyclic AMP-dependent protein kinase A plays a role in the directed migration of human keratinocytes in a DC electric field. *Cell Motility and the Cytoskeleton*, 2001. 50(4): p. 207-217.
48. Brown, M.J., Electric field-directed fibroblast locomotion involves cell surface molecular reorganization and is calcium independent. *The Journal of Cell Biology*, 1994. 127(1): p. 117-128.
49. Ozawa, H., et al., Electric fields stimulate DNA synthesis of mouse osteoblast-like cells (MC3T3-E1) by a mechanism involving calcium ions. *Journal of Cellular Physiology*, 1989. 138(3): p. 477-483.
50. McBain, V.A., J.V. Forrester, and C.D. McCaig, HGF, MAPK, and a Small Physiological Electric Field Interact during Corneal Epithelial Cell Migration. *Investigative Ophthalmology & Visual Science*, 2003. 44(2): p. 540.
51. Shi, G., et al., A novel electrically conductive and biodegradable composite made of polypyrrole nanoparticles and polylactide. *Biomaterials*, 2004. 25(13): p. 2477-2488.
52. Wang, C.H., et al., In-vivo tissue response to polyaniline. *Synthetic Metals*, 1999. 102(1-3): p. 1313-1314.
53. Schmidt, C.E., et al., Stimulation of neurite outgrowth using an electrically conducting polymer. *Proceedings of the National Academy of Sciences*, 1997. 94(17): p. 8948-8953.
54. Li, M.-y., et al., electroactive and nanostructured polymers as scaffold materials for neuronal and cardiac tissue engineering. *Chinese Journal of Polymer Science*, 2007. 25(04): p. 331.
55. Kamalesh, S., et al., Biocompatibility of electroactive polymers in tissues. *Journal of Biomedical Materials Research*, 2000. 52(3): p. 467-478.
56. Guterman E, Cheng S, Palouian K, Bidez P, Lelkes P, Wei Y. Peptide-modified electroactive polymers for tissue engineering applications. In ABSTRACTS OF PAPERS OF THE AMERICAN CHEMICAL SOCIETY 2002, (Vol. 224, pp. U433-U433). 1155 16TH ST, NW, WASHINGTON, DC 20036 USA: AMER CHEMICAL SOC.
57. Kanatzidis, M.G., SPECIAL REPORT. *Chemical & Engineering News*, 1990. 68(49): p. 36-50.
58. Street, G.B. and T.C. Clarke, Conducting Polymers: A Review of Recent Work. *IBM Journal of Research and Development*, 1981. 25(1): p. 51-57.
59. Huang, L., et al., Synthesis and characterization of electroactive and biodegradable ABA block copolymer of polylactide and aniline pentamer. *Biomaterials*, 2007. 28(10): p. 1741-1751.
60. A, M. and M. Reinhardt, Der Eyre-See und sein Becken: von der Sachischen Technischen Hochschule zu Dresden genehmigte Dissertation. *The Geographical Journal*, 1934. 83(6): p. 522.
61. Shreepathi S. Dodecylbenzenesulfonic acid: A Surfactant and dopant for the synthesis of processable polyaniline and its copolymers.
62. Kai, D., et al., Polypyrrole-contained electrospun conductive nanofibrous membranes for cardiac tissue engineering. *Journal of Biomedical Materials Research Part A*, 2011. 99A(3): p. 376-385.
63. Huttmacher, D.W., Scaffold design and fabrication technologies for engineering tissues — state of the art and future perspectives. *Journal of Biomaterials Science, Polymer Edition*, 2001. 12(1): p. 107-124.
64. Giaever, I. and C.R. Keese, Monitoring fibroblast behavior in tissue culture with an applied electric field. *Proceedings of the National Academy of Sciences*, 1984. 81(12): p. 3761-3764.
65. Kerns, J.M., et al., An experimental implant for applying a DC electrical field to peripheral nerve. *Journal of Neuroscience Methods*, 1987. 19(3): p. 217-223.
66. Jaffe, L.F. and M.-M. Poo, Neurites grow faster towards the cathode than the anode in a steady field. *Journal of Experimental Zoology*, 1979. 209(1): p. 115-127.
67. Bassett, C.A.L., R.J. Pawluk, and R.O. Becker, Effects of Electric Currents on Bone In Vivo. *Nature*, 1964. 204(4959): p. 652-654.
68. Bassett, C.A., S.N. Mitchell, and S.R. Gaston, Treatment of ununited tibial diaphyseal fractures with pulsing electromagnetic fields. *The Journal of Bone & Joint Surgery*, 1981. 63(4): p. 511-523.
69. Guimard, N.K.E., J.L. Sessler, and C.E. Schmidt, Toward a Biocompatible and Biodegradable Copolymer Incorporating Electroactive Oligothiophene Units. *Macromolecules*, 2009. 42(2): p. 502-511.
70. Shi, G., Z. Zhang, and M. Rouabhia, The regulation of cell functions electrically using biodegradable polypyrrole-poly lactide conductors. *Biomaterials*, 2008. 29(28): p. 3792-3798.
71. Zhao, M., J.V. Forrester, and C.D. McCaig, A small, physiological electric field orients cell division. *Proceedings of the National Academy of Sciences*, 1999. 96(9): p. 4942-4946.
72. Hardy, J.G., et al., Instructive Conductive 3D Silk Foam-Based Bone Tissue Scaffolds Enable Electrical Stimulation of Stem Cells for Enhanced Osteogenic Differentiation. *Macromolecular Bioscience*, 2015. 15(11): p. 1490-1496.
73. Massoumi, B., et al., AB2 Y-shaped miktoarm star conductive polyaniline-modified poly(ethylene glycol) and its electrospun nanofiber blend with poly(ϵ -caprolactone). *RSC Advances*, 2015. 5(46): p. 36715-36726.
74. Jin, L., et al., Fabrication and characterization of a novel fluffy polypyrrole fibrous scaffold designed for 3D cell culture. *Journal of Materials Chemistry*, 2012. 22(35): p. 18321.